Scale-Free Modeling of Coupled Evolution of Discrete Dislocation Bands and Multivariant Martensitic Microstructure

Valery I. Levitas, S. Ehsan Esfahani, and Iman Ghamarian

Phys. Rev. Lett. **121**, 205701 — Published 15 November 2018

DOI: 10.1103/PhysRevLett.121.205701

Scale-free modeling of coupled evolution of discrete dislocation bands and multivariant martensitic microstructure

Valery I. Levitas,[1,2,3] S. Ehsan Esfahani,[1] and Iman Ghamarian[4]

[1]*Department of Aerospace Engineering, Iowa State University, Ames, IA 50011, USA*
[2]*Departments of Mechanical Engineering and Materials Science & Engineering, Iowa State University, Ames, IA 50011, USA*
[3]*Ames Laboratory, Division of Materials Science and Engineering, Ames, IA 50011, USA*
[4]*Department of Materials Science & Engineering, University of Michigan, Ann Arbor, MI 48109, USA*

(Dated: October 23, 2018)

Scale-free model for the coupled evolution of discrete dislocation bands and multivariant martensitic microstructure is developed. In contrast to previous phase field models, which are limited to nanoscale specimens, this model allows treating nucleation and evolution of martensite at evolving dislocation pileups, twin tips, and shear bands in a sample of an arbitrary size. Model is applied for finite element (FE) simulations of plastic strain-induced phase transformations (PTs) in a polycrystalline sample under compression and shear. Solution explains the one to two orders of magnitude reduction in PT pressure by plastic shear; existence of incompletely transformed stationary state and optimal shear strain for strain-induced synthesis of high pressure phases.

Keywords: Martensitic Phase Transition, Polycrystalline, Strain Softening, Microstructure, Contact Problem

Interaction between PTs and plasticity is one of the fundamental problems in transformational/deformational material behavior and material design [1]. Martensitic PTs usually start at stress concentrators caused by dislocations. In addition to pre-existing dislocations, dislocations may nucleate due to external stresses and internal stresses caused by PT. For plastic strain-induced PTs, the martensite nucleation occurs at dislocations, shear bands, and shear-band intersections that are generated during plastic flow. Plastic deformation reduces PT pressure by a factor of 2 to 10 in comparison with hydrostatic loading for various PTs [2–6]. Recently, reduction in pressure due to plastic shear from 70 to 0.7 GPa was reported for PT from graphite to diamond [7]. Such an extremely strong effect of plastic shear was explained by nucleation at the dislocation pileup [8], which produces a concentration of all components of the stress tensor proportional to the number of dislocations in a pileup. Much more precise simulation for a bicrystal was performed [9–11] using the phase field approach (PFA) to the interaction of PT and discrete dislocations developed in [12, 13].

The main drawback of the traditional PFA is the necessity of numerically resolving the widths of the phase interface and dislocation core, which are $\sim$1 nm. Using 4-5 FEs across an interface required for mesh-independent solutions results in an atomic-size grid. This prevents a numerical treatment of samples exceeding 0.1 - 1 μm. At the same time, the typical initial grain size can be 10-1000 μm or larger.

In some theories [14], the interface width is artificially increased to 1 μm (i.e. by a factor of 1000) while maintaining the same interface energy. However, this leads to a proportional reduction in the stress or temperature hysteresis [4, 15], and the barrierless nucleation in the defect-free crystal occurs very close to the phase equilibrium stress. This is in disagreement with large stress and pressure hysteresis for many PTs [7].

A microscale PFA was suggested in [16, 17] and was applied for the discrete martensitic microstructure evolution in the sample exceeding 100 nm and without an upper limit. We will use this model (see the complete system of equations in [20]) as part of our model for interaction of PTs and discrete dislocations. The order parameter in [16, 17] is the volume fraction of the martensite, c, which causes strain softening and material instability during the PT, the transformation strain localization, and the corresponding discrete martensitic microstructure. This is in contrast to traditional models [18, 19] with strain hardening that produces a smeared description of martensite. The volume fraction of martensitic variants are internal variables rather than order parameters, i.e., they do not describe material instability and do not form martensite-martensite microstructure and interfaces. Material properties are determined by the simplest mixture theory (Eqs. (S.1), (S.5), (S.7)) with the interaction term between austenite and martensite (Eq. (S.2)), which actually causes material instability. The thermodynamic driving forces for all PTs are determined from the thermodynamic laws in Eqs. (S.9) and (S.10). When the driving force exceeds an athermal threshold (Eqs. (S.11) and (S.12)), a linear relationship between the rate of PT and the corresponding net driving force is assumed (Eqs. (S.13) and (S.14)). The model is practically scale-independent because a gradient term is dropped. Although the width of interface, which is equal to a single FE, is mesh-dependent, this weakly affects the morphology of the martensitic microstructure and macroscopic stress-strain curves [15].

In PFA for dislocations [24, 25], scaling up is usually produced by increasing the dislocation height at a fixed Burgers vector, which, however, reduces transformation shear and stress concentration by the same factor. PFA for interaction between discrete dislocations and PTs [12, 13] was utilized at the nanoscale only [9–11].

Our goal is to develop a modeling approach for interaction between PTs and plasticity in large samples that still includes dislocation pileup-type stress concentrators to cause nucleation of the evolving multivariant martensitic regions. In the letter, we suggest the utilization of the contact problem for-

mulation [26, 27] to model multiple dislocations in dislocation pileups and macroscopic shear bands and its combination with the PFA for PT in elastic materials developed in [15–17]. Despite its simplicity, this model effectively reproduces the stress field of a single dislocation (excluding stress divergence) and the solutions to problems on nucleation and evolution of a high pressure phase (HPP) at evolving dislocation pileups in a bicrystal under compression and shear at the nanoscale [9–11]. The model can be used for any sample size exceeding 30-50 nm. It is demonstrated that solutions for stresses and HPP are scale-independent for geometrically similar samples and that the number of dislocations in a pileup increases proportionally to sample size. Problems on two-variant PT and dislocation pileups evolution in a polycrystalline sample under compression and shear are solved and utilized for the interpretation of drastic reduction in PT pressure due to plastic deformations [2–7] and other related phenomena.

Dislocations via contact problem. By definition [28, 29], a dislocation represents a cut in an elastic continuum and relative sliding of two sides of the cut by the Burgers vector $\boldsymbol{b}$. Likewise, multiple dislocations along the same slip surface, which can be considered to be continuously distributed, can be defined by the relative sliding $\boldsymbol{u}_s$. Furthermore, the traction and normal displacements across the cut are continuous. Similar conditions can be reproduced by the solution of a contact problem [26, 27] between two deformable bodies. The tangential to the contact surface displacements, i.e. relative sliding $\boldsymbol{u}_s$, is determined by the constitutive equations. We define the following general sliding (slip) rule

$$\dot{\boldsymbol{u}}_s = \begin{cases} 0 & \text{if} \quad f(\boldsymbol{\tau}) < 0 \\ \boldsymbol{q}(\boldsymbol{\tau}) & \text{if} \quad f(\boldsymbol{\tau}) \geq 0 \end{cases}, \tag{1}$$

where $f = 0$ is the limit surface in the space of the shear stress $\boldsymbol{\tau}$ within a slip plane, which characterizes athermal resistance to dislocation motion and within which sliding is impossible, and $\boldsymbol{q}$ is the function that determines the kinetics of slip. These functions may include anisotropy, rate and normal stress dependence, and other features from the theory of discrete or continuous dislocations or crystal plasticity [28–30]. In particular, sliding can be allowed along the known slip directions within a slip plane, governed by a resolved shear stresses along these directions, and with some interaction terms between slip rates along different slip systems. Because our current applications will be 2D, we simplify the sliding rule as

$$\dot{\boldsymbol{u}}_{\boldsymbol{s}} = \begin{cases} 0 & \text{if} \quad |\tau| < \tau_c \\ k\tau & \text{if} \quad |\tau| \geq \tau_c \end{cases}, \tag{2}$$

where τ_c is the athermal threshold, and $k > 0$ is a scalar, which is determined from the condition $|\tau| = \tau_c$, which corresponds to the main equilibrium equations for continuous dislocation distribution [28, 29]. The only spatial scale parameter, the Burgers vector, does not need to be resolved numerically; i.e. the model is scale-independent and can be applied to an arbitrary large sample.

Expressing equations for continuous distributions of dislocations along the chosen slip surfaces in terms of formulation of a contact problem allows us to utilize well developed FE method codes for the solution of contact problems to simulate continuous dislocation evolution along the discrete slip surface. By combining the contact problem with the model for a scale-free multivariant martensitic PTs presented in [20] (i.e., solving Eq. (2) along with Eqs. (S.4)-(S.17)), we can describe the interaction of PTs and discrete dislocation pileups along the prescribed slip systems. The critical shear stress τ_c generally varies for different phases. If part of a slip plane coincides with the phase interface, i.e. one side of the contact couple belongs to one phase and another side belongs to an other phase, the smaller τ_c is used.

PTs between low-pressure phase (LPP) bcc (austenite) and HPP bct (martensite) are considered. The material parameters are: the difference in the thermal energy between HPP and LPP $\Delta G^\theta = 1.0$ GPa, the phase equilibrium pressure $p_e = 10$ GPa, and the lattice instability pressure for the LPP $p_{cr} = 20$ GPa; see also [20]. Quadratic plane strain FEs, straight edge dislocations, the same τ_c for both phases, and two martensitic variants are considered.

The model is implemented in Abaqus FE code through a corresponding UMAT subroutine [27]. The mesh generation, the shape and orientation of the grains and the slip systems are facilitated via DREAM.3D [31] and MTEX [32]. Bcc crystal deforms mainly along 12 slip systems $\{110\}\langle 111\rangle$ in 3D, but $\{112\}\langle 111\rangle$ may also be operative [34]. The only way to make simulations consistent with the plane strain treatment is to select $\{112\}\langle 111\rangle$ slip systems, which are inherited by a bct crystal. Then, for all grain orientations, the Bunge-Euler angles [33] are $\varphi = 135^\circ$, $\varphi_2 = 0^\circ$, and φ_1 (a rotation about the out-of-plane normal). Specific slip systems and the values of φ_1 are shown in all figures. The angle between $(2\bar{1}\bar{1})[111]$ and $(211)[\bar{1}11]$ slip systems is 70.52°.

When in the contact problem $u_s = b$ is imposed along part of a contact line in a sufficiently large sample, producing separated positive and negative dislocations, the stress fields are in good agreement with the analytical solution for a single dislocation [28] for $|x| \geq 0.3b$. It is proven that by changing the mesh density, regularity, and the element type, the all following solutions are practically mesh-independent.

First, we solve the problem on *PT at the dislocation pileup in a bicrystal*, for the same conditions as in [9] in which the nanoscale PFA was utilized. Consider a sample which consists of two rectangular crystals, both of the size $h \times L$ =20×25, in which the PT and/or the contact problem for the dislocation pileup are solved (Fig. 1). Two rectangles with the size of 50×5 at the top and bottom of the bicrystal simulate the elastic accommodations of the surrounding grains. We chose $\tau_c = 1.0$ GPa. In the presence of one dislocation, at the center of a sample and under hydrostatic loading, the lowest hydrostatic pressure at which the HPP nucleates is $p_h = 14.70$ GPa; this is close to 15.75 GPa reported in [9].

In Figs. 1 and 2, the top edge of the sample is subjected to a homogeneous Cauchy (true) compressive stress σ_n and uni-

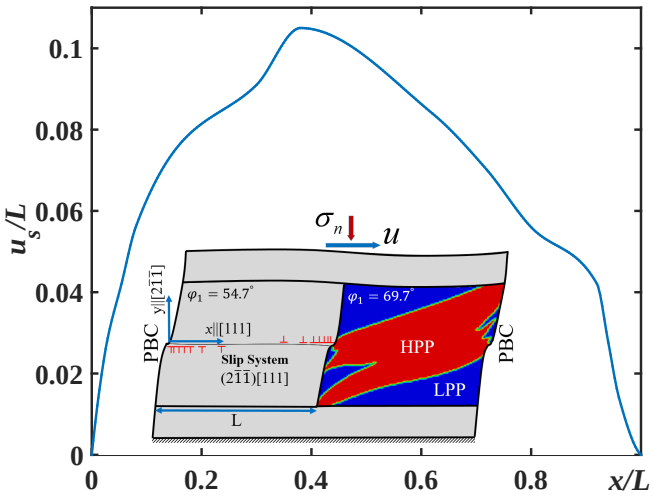

FIG. 1. Distribution of normalized sliding displacements u_s/L along the slip system in the left grain vs. normalized distance x/L. Results for $L = 25$ nm and L increased by factors of 10, 10^2, and 10^3 coincide, i.e. solutions for stress, strain, and PT are independent of scale. Inset: Geometry, loading conditions, and stationary solution for volume fraction of HPP c and dislocations in a bicrystal under fixed compression $\sigma_n = 3.05$ GPa and shear $\gamma = 0.2$. Dislocation signs are placed at points corresponding to the integer values of number of dislocations $n = u_s/b$.

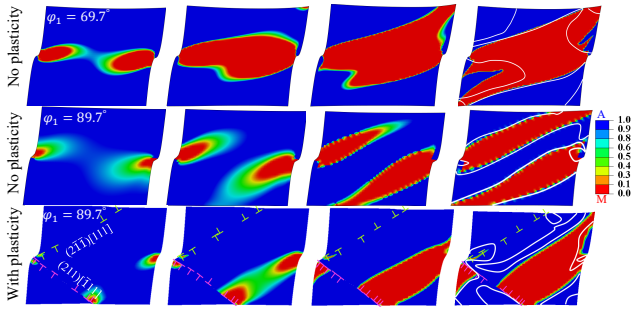

FIG. 2. Nucleation and evolution of the HPP in the right grain at fixed $\gamma = 0.2$ and $\sigma_n = 3.05$ GPa (a) without plasticity for $\varphi_1 = 69.7°$ and (b) for $\varphi_1 = 89.7°$, as well as (c) with plasticity for $\varphi_1 = 89.7°$. White isolines for the stationary solutions correspond to the local phase equilibrium condition, $\boldsymbol{\sigma} : \boldsymbol{\varepsilon}_t = \Delta G^\theta = 1.0$ GPa.

form horizontal displacement, u, presented by macroscopic shear $\gamma = u/h$, both constant in time, where h is the height of the grains; periodic boundary conditions (PBC) for displacements are implemented on the lateral edges; and the bottom edge is fixed. These fast loading conditions are the same as in [9]. The PT without dislocations in the right grain is studied when a single horizontal contact surface as the slip plane for modeling dislocation activity is introduced in the left grain. For characterization of the PT in 2D, the pressure is defined as $p = -0.5(\sigma_x + \sigma_y)$. Without shear strain, the stress $\sigma_n = 3.05$ GPa results in an averaged pressure of 2.0 GPa over each grain. With the increasing shear γ, the contact surfaces start slipping, producing an increasing number of couples of positive and negative dislocations. Several dislocations pile up at the grain boundary, producing steps from both sides of the bicrystal. The stationary solution for $\gamma = 0.2$ contains a pileup of 7 dislocations, the same number as in [9]. Thereafter, the PT is permitted in the right grain, similar to [9]. Due to the high-stress concentrations at the tip of the dislocation pileup, two HPP regions nucleate, grow, and coalesce. The final volume fraction of HPP averaged over the right grain is $\tilde{c} = 0.58$. In [9], $\tilde{c} = 0.51$, and the morphology of the HPP region is quite close to what is obtained here (see Fig. 2a and Fig. S1 in [20]). Thus, our model is effective in reproducing results from the much more sophisticated nanoscale model in [9]. Due to the volume reduction during PT, the averaged pressure over both grains reduced to a stationary value $\bar{p} = 0.07$ GPa. This is more than two orders of magnitude lower than the PT pressure of 14.7 GPa under hydrostatic loading. This conceptually proves the ability of our model to describe the drastic reduction in the PT pressure due to plastic shear obtained in experiments [2–7]. Figs. 2a and b show that the morphology strongly depends on the grain orientations.

Variation of sample size, L, for geometrically similar samples under the same σ_n and γ by three orders of magnitude illustrates that the curve of the normalized sliding displacement u_s/L vs. x/L, as well as the stress, strain, and volume fraction of the HPP fields are independent of L. Thus, our model is indeed scale-independent.

Next, we allow dislocation activity in the right grain ($\varphi_1 = 89.7°$) by introducing two slip systems with $\pm 35.26°$ to the x-axis (Fig. 2c) and start the PT and sliding within right grain after reaching a stationary dislocation solution in the left grain. Due to rate-independent dislocation kinetics (2), dislocations are much faster than the PT, and the corresponding stress relaxation suppresses the PT. Three nuclei instead of two are observed in Fig. 2c; two of them coalesce. These nuclei do not cross the slip planes because tensile stresses in the regions with missing atomic planes produce athermal interface friction. In fact, in addition to the tip of the dislocation pileup, strong compressive stress concentrator near the extra planes of dislocations promotes the nucleation and stabilization of HPP, and should be considered as a new nucleation site not mentioned in the literature. In total, the HPP region ($\tilde{c} = 0.35$) is smaller than the one in Fig. 2b ($\tilde{c} = 0.48$). Nonetheless, similar to the nanoscale PFA [9, 10], we are able to find such combinations of loading conditions that the PT wins its competition with the plasticity.

When the elastic properties of the material do not change during the PT and the contribution from the surface energy is neglected, the following phase equilibrium condition for each point of a sharp interface should be valid [10, 11, 35]:

$$\boldsymbol{\sigma} : \boldsymbol{\varepsilon_t} = \Delta G^\theta, \tag{3}$$

in which $\boldsymbol{\sigma} : \boldsymbol{\varepsilon_t}$ is the transformation work ($\boldsymbol{\varepsilon_t}$ is the transformation strain tensor). The isolines corresponding to Eq. (3) based on the local stress tensor field are plotted in Fig. 2. For most interfaces, the condition in Eq. (3) is met, similar to the nanoscale PFA [10, 11]. Surprisingly, the plastic strain does

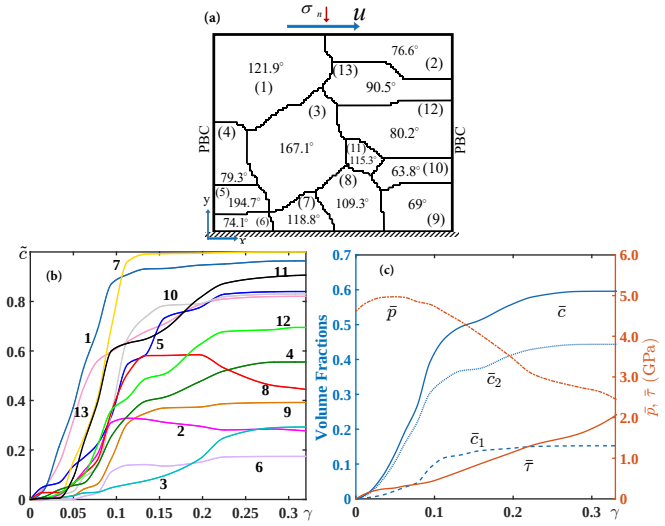

FIG. 3. (a) The grain structure of the polycrystal with shown φ_1 angles loaded by fixed $\sigma_n = 6.05$ and shear strain rate of $0.004\ s^{-1}$, (b) evolution of the averaged volume fraction of the HPP, $\tilde{c}$, in each grain, and (c) evolution of pressure, shear stress, and volume fraction of the HPP $\bar{c}$ as well as each martensitic variants $\bar{c}_i$ averaged over the sample vs. the macroscopic shear strain.

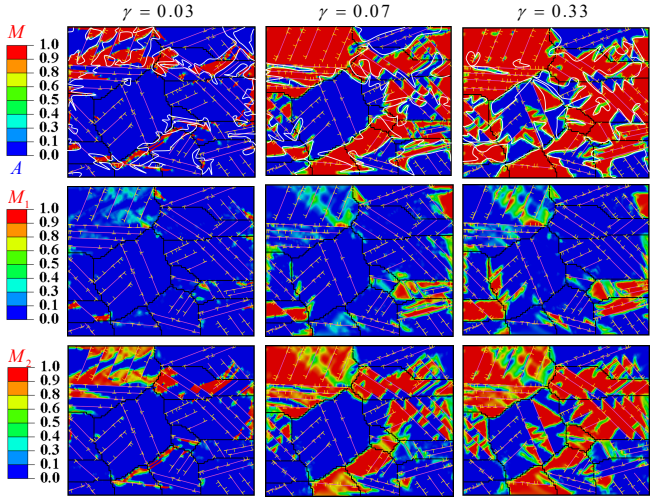

FIG. 4. Evolution of dislocations, the HPP (a), and two martensitic variants (b and c) under stress fixed σ_n =6.05 and shear strain rate of $0.004\ s^{-1}$.

not appear in Eq. (3); however, plasticity contributes indirectly by changing local stresses.

Coupled dislocation and PT evolution in a polycrystalline aggregate shown in Figs. 3a and 4 is studied at $\tau_c = 0.3$ GPa, fixed $\sigma_n = 6.05$, and slow shear straining with the rate of $0.004\ s^{-1}$. Location, number of slip bands, and spacing between them are determined by initial heterogeneities of the microstructure (defects and composition) and internal stresses and are chosen arbitrarily. Nucleation of HPP occurs mostly near the extra planes of dislocations in the same grains and near to the tip of dislocation pileups in the neighboring grains. For most interfaces, the phase equilibrium condition (3) is met. This confirms the necessity of excluding plastic work from the Eshelby driving force for the interface propagation debated in [35]. The averaged volume fraction of the variant 2 is larger than for variant 1. Due to the different orientations, sizes, and positions of grains, a very heterogeneous volume fraction of the HPP in different grains is observed (Fig. 3b). The smallest volume fraction is in the grains located at the corners (grains 6, 2, and 9); however, the PT is very pronounced in a large corner grain 1. The PT in most grains reaches or nearly reaches the stationary state , and reverse PT occurs in grains 2 and 8.

The results for some parameters averaged over the entire sample are shown in Fig. 3c. After a small initial growth from 4.7 to 5 GPa, the averaged pressure drops to 2.4 GPa during the shear due to the reduction in volume throughout the PT. The shear stress increases to 2.05 GPa due to the increasing number of dislocations as well as the back stresses due to dislocation pileups at grain boundaries and stress heterogeneities in various grains. Thus, the shear stresses play a more active role than the pressure with a PT progression. Based on the curves for $\bar{c}_i$ and $\bar{c}$, *PT reached a stationary state and further increase in shear is not productive*. This result corresponds to the existence of the stationary, incompletely-transformed states for strain-induced PTs [8, 36, 37] and the concept that plastic shear should be optimal rather than as large as possible [36].

Note that both for bicrystal and polycrystal, the *phase equilibrium condition (3) is also met for the stresses averaged over the entire sample*. This finding, along with the results in Fig. 3c, is important for the computational development of the model for polycrystalline aggregate, which is required for macroscale modeling of the behavior of a sample compressed and sheared in traditional and rotational diamond anvils [38, 39]. A greatly simplified kinetic model [8] is currently used.

Thus, a scale-free model for the coupled evolution of discrete dislocation bands and multivariant martensitic microstructure is developed. As a thin twin in [29] and shear crack in [40] are presented as dislocation pileups, our model includes them as well. Because our approach is based on slip displacements, it can be applied to macroscopic shear bands without referring to dislocations as well. The independence of the solutions of the sample size is demonstrated. Despite its simplicity, the model reproduces well solutions obtained with the nanoscale PFA [9–11]. The plastic strain-induced PT in a polycrystalline sample under compression and shear is simulated. The solution explains a drastic reduction in PT pressure due to plastic deformations [2–7]; the existence of an incompletely-transformed stationary state; and optimal shear strain for strain-induced synthesis of HPPs. The simplest phase equilibrium condition (3), which does not contain plastic work and surface energy, is met for the entire sample and most of the interfaces.

Acknowledgments: Supports of NSF (CMMI-1536925),

ARO (W911NF-17-1-0225), ONR (N00014-16-1-2079) and the ISU (Vance Coffman Faculty Chair Professorship) are gratefully acknowledged. The simulations were performed at XSEDE, allocation TG-MSS140033.

[1] Olson, G.B., (1997). Computational design of hierarchically structured materials. *Science*, 277(5330): 1237-42.

[2] Levitas, V. I. , Shvedov L. K., (2002). Low pressure phase transformation from rhombohedral to cubic BN: experiemnt and theory *Phys. Rev. B.* 65: 104109

[3] Blank, V. D., Estrin, E. I., (2014). Phase Transitions in Solids under High Pressure, *CRC Press*, Boca Raton.

[4] Ji, C., Levitas, V. I., Zhu, H., Chaudhuri, J., Marathe, A., Ma, Y., (2012). Shear-induced phase transition of nanocrystalline hexagonal boron nitride to wurtzitic structure at room temperature and lower pressure. *Proc. Natl. Acad. Sci. U S A.* 109(47): 19108-12.

[5] Perez-Prado, M. T., Zhilyaev, A. P., (2009). First experimental observation of shear induced hcp to bcc transformation in pure Zr *Phys. Rev. Lett.* 102: 175504

[6] Srinivasarao, B., Zhilyaev, A. P., Prez-Prado, M. T., (2011). Orientation dependency of the alpha to omega plus beta transformation in commercially pure zirconium by high-pressure torsion *Scripta Mater.* 65 (3): 241-244

[7] Gao, Y., Ma, Y., An, Q., Levitas, V., Zhang, Y., Feng, B., Chaudhuri, J., Goddard III, W.A., (2018). Shear driven formation of nano-diamonds at sub-gigapascals and 300 K. *arXiv preprint arXiv*:1805.11239.

[8] Levitas, V. I, (2004). High-pressure mechanochemistry: conceptual multiscale theory and interpretation of experiments. *Phys. Rev. B.* 70:184118

[9] Levitas, V. I., Javanbakht, M., (2014). Phase transformations in nanograin materials under high pressure and plastic shear: nanoscale mechanisms. *Nanoscale.* 6: 162-166.

[10] Javanbakht, M., Levitas, V. I., (2016). Phase field simulations of plastic strain-induced phase transformations under high pressure and large shear. *Phys. Rev. B.* 94: 214104.

[11] Javanbakht, M., Levitas, V. I., (2018). Nanoscale mechanisms for high-pressure mechanochemistry: a phase field study. *J. Mater. Sci.* 53: 13343-63.

[12] Levitas, V. I., Javanbakht, M., (2015). Interaction between phase transformations and dislocations at the nanoscale Part 1: General phase field approach. *J. Mech. Phys. Solids* 82: 287-319.

[13] Javanbakht, M., Levitas, V. I., (2016). Interaction between phase transformations and dislocations at the nanoscale. Part 2: Phase field simulation examples. *J. Mech. Phys. Solids*. 82:164-185

[14] Steinbach, I, Apel, M., (2006). Multi phase field model for solid state transformation with elastic strain. *Phys. D.* 217: 15360.

[15] Esfahani, S. E., Ghamarian, I., Levitas, V. I., Collins, P. C., (2018). Microscale phase field modeling of the martensitic transformation during cyclic loading of NiTi single crystal. *Int. J. Solids Struct.* 146: 80-96.

[16] Levitas, V. I., Idesman, A. V., Preston, D. L., (2004). Microscale simulation of martensitic microstructure evolution. *Phys. Rev. Lett.* 93: 105701.

[17] Idesman, A. V., Levitas, V. I., Preston, D. L., Cho, J. -Y., (2005). Finite element simulations of martensitic phase transitions and microstructures based on a strain softening model. *J. Mech. Phys. Solids.* 53: 495-523.

[18] Lagoudas, D. C., (2008). Shape memory alloys. *Science and Business Media, LLC*.

[19] Lexcellent, C. (2013). Shape-memory alloys handbook. *John Wiley & Sons*.

[20] See Supplemental Material at [URL will be inserted by publisher] for the complete system of equations and comparison of solution with the nanoscale model in [9], which includes Refs. [21–23].

[21] Arghavani, J., Auricchio, F., Naghdabadi, R., Reali, A., Sohrabpour, S., (2010). A 3-D phenomenological constitutive model for shape memory alloys under multiaxial loadings. *Int. J. Plast.* 26:976-91.

[22] Lagoudas, D., Hartl, D., Chemisky, Y., Machado, L., Popov, P., (2012). Constitutive model for the numerical analysis of phase transformation in polycrystalline shape memory alloys. *Int. J. Plast.* 32:155-83.

[23] Saleeb, A. F., Padula, S. A., Kumar, A., (2011). A multi-axial, multimechanism based constitutive model for the comprehensive representation of the evolutionary response of SMAs under general thermomechanical loading conditions. *Int. J. Plast.* 27:655-87.

[24] Wang, Y. U., Jin, Y. M., Cuitino, A. M., Khachaturyan, A. G., (2001b). Nanoscale phase field microelasticity theory of dislocations: model and 3D simulations. *Acta Mater.* 49: 1847-57.

[25] Jin, Y. M., Khachaturyan, A. G., (2001). Phase field microelasticity theory of dislocation dynamics in a polycrystal: model and three-dimensional simulations. *Philos. Mag.* 81: 607-16.

[26] Wriggers, P. (2006). Computational Contact Mechanics. *Springer-Verlag Berlin Heidelberg*.

[27] Abaqus 6.14 Analysis User's Manual, contact problem: 37.1 Mechanical contact properties, especially 37.1.5 Frictional behavior, SIMULIA, Providence, RI (2014).

[28] Hirth, J. P., Lothe, J., (1982). Theory of dislocations. New York: John Wiley & Sons.

[29] Boyko, V., Garber, R., Kossevich, A., (1997). Reversible Crystal Plasticity, *AIP*, New York.

[30] Asaro, R. J., 1983. Crystal plasticity. *J. Appl. Mech.*, 50(4b), 921-934.

[31] Groeber, M. A., Jackson, M. A., (2014). DREAM. 3D: a digital representation environment for the analysis of microstructure in 3D. *Integr. Mater. Manuf. Innovation*, 3(1): 5.

[32] Bachmann, F., Hielscher, R., Schaeben, H., (2010). Texture analysis with MTEX-free and open source software toolbox. *In Solid State Phenomena* 160: 63-68.

[33] Kocks, U. F., Tome, C. N., Wenk, H. R., Beaudoin, A. J., (2000). Texture and anisotropy. *Cambridge University Press*.

[34] Serenelli, M. J., Bertinetti, M. A., Signorelli, J. W., (2010). Investigation of the dislocation slip assumption on formability of BCC sheet metals. *Int. J. Mech. Sci.*, 52: 1723-34.

[35] Levitas, V. I., (2002). Critical thought experiment to choose the driving force for interface propagation in inelastic materials. *Int. J. Plast.* 18: 1499-525.

[36] Levitas, V. I., Zarechnyy, O. M., (2006). Kinetics of strain-induced structural changes under high pressure. *J. Phys. Chem. B*. 110: 16035-46.

[37] Straumal, B. B., Kilmametov, A. R., Ivanisenko, Y., Mazilkin, A. A., Kogtenkova, O. A., Kurmanaeva, L., Korneva, A., Ziba, P., Baretzky, B., (2015). Phase transitions induced by severe plastic deformation: steady-state and equifinality. *Int. J. Mater. Res.*, 106(7): 657-64.

[38] Levitas V. I., Zarechnyy, O., (2010). Modeling and simulation of strain-induced phase transformations under compression and torsion in a rotational diamond anvil cell. *Phys. Rev. B* 82:

174124.

[39] Feng, B., Levitas, V. I., (2016). Effects of the gasket on coupled plastic flow and strain-induced phase transformations under high pressure and large torsion in a rotational diamond anvil cell. *J. Appl. Phys.* 119(1), 015902.

[40] Rice, J. R., (1968). In: Fracture: an advanced treatise. Vol. 3, 2: 191-311, Liebowitz, H. (Ed.), Academic Press, NY, London.